

行政院國家科學委員會補助專題研究計畫成果報告
無線正交分頻多重進接頻道使用技術研究及全系統整合(I)
Wireless OFDMA Channel Utilization Techniques Research and Full-System Integration

計畫編號：NSC 91-2219-E-009-008

執行期限：91年8月1日至92年7月31日

主持人：林大衛 交通大學電子工程學系 教授

計畫參與人員：吳俊榮、林孟亭、何玉屏、李明哲、林筱晴、陳盈縈 交通大學電子工程學系 研究生

摘要

本計畫為一整合型計畫之子計畫，擬為期三年，其中最主要的工作是基於 IEEE 802.16a 標準，研究正交分頻多重進接(OFDMA)在作無線行動通訊服務之用時的傳收技術，並將各子計畫之實現成果予以整合。此外亦對相關之多載波調變技術，從事基礎性的研究。本報告係針對第一年之成果，其中我們除了了解 IEEE 802.16a 標準之相關規範，並為了系統模擬與整合之需，探討了其中幾項主要的傳收技術，特別是同步及通道編解碼技術。我們亦考慮了適用於系統實現的數位訊號處理平台。此外，在多載波調變的基礎性研究方面，我們探討了使用奇值分解(SVD)的多載波調變在多路徑淡化通道中的性能及其與使用離散傅立葉轉換(DFT)者的差異。

關鍵詞：IEEE 802.16a、正交分頻多重進接、正交分頻多工調變、時間同步、頻率同步、通道編解碼、基於奇值分解之多載波調變

Abstract

This subproject is a part of an integrated project. It is intended for three years, wherein the major work is to base on the IEEE 802.16a standard and research into the OFDMA (orthogonal frequency-division multiple access) transceiving technologies for wireless mobile communication service. It is also responsible for integrating the implementation results of all the subprojects. Further, it also considers some fundamental issues concerning multicarrier modulation. This report is concerned with the first year's results. In this year, besides understanding the specifications of IEEE 802.16a, we studied several key transceiving technologies for the need of system simulation and integration, which include, especially, synchronization and channel coding techniques. We also considered the digital signal processing platform suitable for system implementation. In addition, in fundamental research concerning multicarrier modulation we investigated the performance in multipath fading channel of SVD (singular value decomposition)-based multicarrier modulation and its difference with that based on DFT (discrete Fourier transform).

Keywords: IEEE 802.16a, Orthogonal Frequency-Division Multiple Access (OFDMA), Orthogonal Frequency-Division Multiplexing (OFDM), Time Synchronization, Frequency Synchronization, Channel Coding, SVD-Based Multicarrier Modulation

目錄 Table of Contents

一、計畫緣由與目的	1
二、結果與討論	1
A. 資料組裝與解組裝(data framer/deframer)及位元映射與解映射(bit mapper/demapper)	1
B. 通道模擬	2
C. 同步技術	2
D. 通道估計與等化	3
E. 通道編解碼	3
F. 數位訊號處理實現平台之考慮	4
G. 基於奇值分解之多載波調變	4
三、參考文獻	5
四、圖表	6
五、計畫成果自評	8
六、可供推廣之研發成果資料表	8
七、附錄	11

一、計畫緣由與目的

本計畫為一整合型計畫之子計畫，擬為期三年。該整合型計畫一主要目標是基於 IEEE 802.16a 標準，研究正交分頻多重進接(OFDMA)在作無線行動通訊服務之用時的傳收技術，並將各分項技術作數位訊號處理器(DSP)軟體或 FPGA 硬體實現。本子計畫負責其中若干傳收技術之研究，並負責將各子計畫之分項實現成果予以整合。此外，本子計畫亦對多載波調變相關技術，從事較基礎性的研究。

IEEE 802.16a 標準容許 FDD (frequency-division duplexing)及 TDD (time-division duplexing)兩種雙工方式。鑒於未來的高速無線通訊很可能具有雙向不對稱的傳輸率，我們決定考慮 TDD 雙工，並兼顧上行與下行(或稱上鏈與下鏈)兩方向傳輸技術的研究。IEEE 802.16a 之 OFDMA 實體層(PHY layer)傳輸系統之基本架構，在上行與下行二個方向相似，概略如圖一所示。圖中以陰影突顯之組件由本子計畫負責實現。由於本子計畫要負責全系統的整合，也由於軟體(或硬體)實現的工作係於第二年度中(92/8-93/7)才要陸續開始，故本子計畫在第一年的研究未限於陰影所示之組件，而是求能對整個系統有所掌握。

以下我們分段陳述本年的研究結果，其中包括 IEEE 802.16a 傳收系統組件的研究、系統實現平台的考慮、及多載波調變技術的基礎性研究。在傳收系統組件中，我們對同步與通道編解碼技術作了特別深入的探討。

二、結果與討論

A. 資料組裝與解組裝(data framer/deframer)及位元映射與解映射(bit mapper/demapper)

圖二所示為 IEEE 802.16a OFDMA TDD 訊框(frame)中，上下行時間的分配與資料結構的示意。我們整理了標準中有關資料組裝與位元映射的規範。其中比較特別的是子通道(subchannels)與嚮導載波(pilot carriers)的分配安排。

對下鏈傳輸而言，嚮導載波的安排比較簡單。在總共 2048 個次載波中，最左與最右端共 345 個空載波(null carriers)。中間 1703 個次載波中，則包含 1536 個資料載波，166 個嚮導載波與 1 個直流載波。嚮導載波中又可分為 32 個固定位置與其餘的浮動位置。固定位置的安排可以查得知，浮動位置的安排則是透過公式計算，使嚮導載波在不同的 OFDM 訊號中，平均的分散在不同的位置。這樣的安排有助於估計隨時間而變的通道狀況。

上鏈的情況比較複雜。扣除左右端的空載波後，剩下的次載波先均分為 32 組子通道。在每個子通道的 53 個次載波中，有 1 個固定位置嚮導載波及 4 個浮動位置嚮導載波，其餘均為資料載波。

這些次載波安排的特性，對使用嚮導載波的運算，如同步與通道估計，是不可或缺的資訊。至於資料組裝與解組裝及位元映射與解映射的實現，比之同步、等化、與通

道解碼等，並無理論上的議題須先解決，且其功能似較宜以軟體達成。

B. 通道模擬

在 IEEE 802.16a 標準中提到幾個固定式無線傳輸的通道模型。但由於我們亦考慮行動狀態下的傳輸，故需再自文獻中搜尋合用的模型。基本上，這些模型需適用於寬頻傳輸。所以，如 3GPP WCDMA 等行動寬頻傳輸系統的通道模型就是可以在本研究中考慮使用的。在 IEEE 802.16e 及 802.20 兩團體中，對於通道模型也有一些討論，我們將繼續注意之。例如在下述關於同步的研究中，我們曾使用的 ESTI Vehicular A 通道模型，亦是 802.16e 中被人提出的一個模型。

無線通道的模擬，其計算量極大。我們過去的經驗顯示，其 DSP 軟體模擬是相當需花力氣來設計與完成的。由於 DSP 的速度在不斷提昇中，且具有高度可程式性，似乎比 FPGA 容易來模擬不同的通道狀況，所以我們暫以使用 DSP 為優先。但我們預定將在第二年的研究中，對使用 DSP 與使用 FPGA 的優劣，加以進一步的比較。

C. 同步技術

對 OFDM 系統而言，接收端收到的訊號如果在時間與頻率上與系統預期的值不同時，都會造成解調動作的干擾。時間上的差異會造成解調訊號相位偏差，或甚至造成相鄰段落訊號的干擾(ISI)；而頻率的差異則會破壞次載波之間的正交性，並且導致次載波間的相互干擾(ICI)。為了克服類似問題的技術通稱為同步技術。

一般而言，OFDM 系統採用的同步技術主要可分為三大類：利用間隔區間(guard interval)重複性、利用空載波不含訊號的特性、利用已知的前置(preamble)或嚮導載波(pilot carriers)。針對本計畫所依據的 IEEE 802.16a 系統特性，我們為上鏈與下鏈傳輸設計了不同的同步動作，詳可見[1]，另亦可參附錄 A(會議論文初稿)。

在下鏈傳輸的同步中，我們共設計四級的同步動作。第一、二級是用 OFDM 系統特有的間隔區間估計到達時間與頻率差異的分數部分。這裡所謂的間隔區間，乃是由 OFDM 的段落訊號中，重複尾端部分的訊號並且置於段落訊號的起始位置。因此，間隔區間本身在接收到的訊號列中即可呈現重複的特性。我們採用這樣的方法作為第一、二級的處理，可以在不依靠任何已知訊號(如 pilot 或 preamble)的情況下，得到基本的估計值。第三級利用 802.16a 規範的空載波及部分的 pilot carriers 判斷頻率差異的整數部分。第四級則利用前置訊號判斷訊框(frame)開始時間。至此用戶端(subscriber)應能的掌握訊框開始時間，OFDMA 符號(symbols)開始時間與頻率差異值。

至於上鏈的同步動作，我們針對 802.16a 規範的前置訊號，設計兩種不同的同步方式：時域以及頻域相關性分析(time-domain or frequency-domain correlation)。上鏈的前置與下鏈不同的地方在於，前者包含了所有的次載波，而後者僅包含部分次載波(參圖二)。利用時域的同步是由基地端產生已知的前置訊號，並與接收到的訊號進行相關性的分析，當相關性最高時，即為訊框大概的開始時間；而利用頻域的同步則是將收到的訊號經過 DFT 處理，所得的結果再與已知的前置訊號頻域進行相關性的分析。我們的模擬顯示，利用時域的同步方法，不但效果較好，複雜度也比較低。

D. 通道估計與等化

本計畫在第一年中，僅對通道估計與等化的方法進行 survey，將在第二年中，對通道估計與等化技術及其實現，作深入的探討。在 IEEE 802.16a 規格中，上行與下行兩方向的次載波使用方式相當不對稱，所以兩方向的通道估計與等化方法以及其 DSP 實現，需要個別的研究與設計。一般而言，多載波傳輸之下的等化可並用時域等化與頻域等化，但在通道的 impulse response 或 delay spread 較 OFDM symbol 的 guard interval 為短時，可省略時域等化。本計畫即考慮僅做頻域等化，此亦為一般無線 OFDM 傳輸之研究所考慮者。

E. 通道編解碼

在 IEEE 802.16a 系統中，通道編解碼是由三個部分所構成：里德-所羅門碼 (Reed-Solomon code, or RS code)、迴旋碼(convolutional code)以及位元間插器(bit interleaver)，如圖三所示。迴旋碼用於修復雜訊干擾造成的失真，RS code 用於修復相連的錯誤(burst error)，交換器則能更進一步的打散連續的錯誤。這些元件都是無線數位通訊中常用的編解碼工具。

在通道碼的使用中，802.16a 還運用了三個特別的機制：縮短(shortening)、穿孔(puncturing)與去尾(tail-biting)。實際上 802.16a 所用的迴旋碼與 RS code 都只有一種，但透過這三種機制，就提供了六種不同的編碼速率，參表一。經過縮短與穿孔的 RS code 可提供不同的段落長度(block size)與除錯能力；經過穿孔與去尾的迴旋碼則提供了不同的編碼速率，並保持段落的完整性。

我們已針對這些 802.16a 中的編碼規定，設計了相對應的解碼方法。縮短、穿孔、以及 IEEE 802.16a 特別的 RS code 產生多項式(generator polynomial)都相當容易作對應的解碼處理。比較困難的是去尾編碼與位元間插的處理。關於去尾編碼，最直接的解碼法的對所有可能的開始與結束狀態(states)解碼，再從其中找到最佳者；其複雜度是一般解碼法的 N 倍，其中 N 為狀態數目。我們採用[2]與[3]的思路，僅用一個開始狀態，但將 trellis 延伸一段長度，其中延伸部分的內容係重複原始 trellis 的內容，如此就可收斂到一個不錯的解碼結果。關於位元間插，對應的最佳解碼法之複雜度不可想像。我們參考[4]-[6]的想法，設計了次佳解碼法，實驗顯示其與最佳解碼法間的效能差異僅約 0.1-1.0 dB。

我們在加成性白色高斯通道下和淡化通道下分別模擬了里德-索羅門碼，迴旋碼，和串接碼，並把模擬之結果與一些分析的結果做比較，包含在加成性白色高斯通道下 IEEE 802.16a 的編碼增益需求值，用 Shannon 極限求出的編碼極限值，及用最短碼字間距求出的增益值。在加成性白色高斯通道下，里德-索羅門碼和迴旋碼的編碼增益值幾乎達到理論值，但整體的編碼增益值離理論值或 IEEE 802.16a 的編碼增益需求值卻有很大的差距。這與能找到的 802.16a Task Group 之文獻資料相吻合。我們預測在更高的號雜比下，實際的編碼增益值會比較接近理論計算出的編碼增益值。詳可見[7]，另亦可參附錄 B(會議論文初稿)。

F. 數位訊號處理實現平台之考慮

在系統整合方面，首先要完成的是實作平台的選定。其中牽涉的層面很廣：如硬體速度快慢、硬體資源是否充足、編譯與可程式化(programmable)的難易度、還有其價格以及其與現有資源是否可整合等問題。在經過詳細的討論與調查之後，我們選擇了混合 DSP 晶片與 FPGA 的系統，以提供具高度彈性的實現平台。這是因為我們的系統大部分的運算是希望以高效能的 DSP 晶片完成，但某些高運算複雜度的傳收系統組件(如無線通道模擬與通道解碼)，可能須使用 FPGA 才能作較高速度的實現。

Innovative Integration 公司有一系列名為 Quixote 的系統。此系統同時包含具高運算效能的 TI DSP 晶片 TMS320C6416 與 Xilinx FPGA 晶片 Virtex-II，並可與我們既有的 DSP 設備互連。我們將在第二年的計畫中，嘗試使用此設備。

G. 基於奇值分解之多載波調變

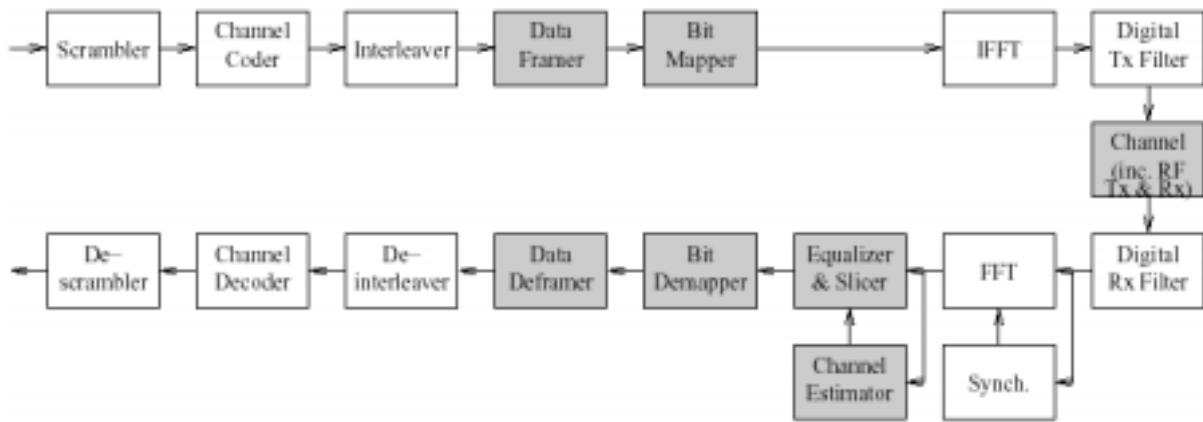
由圖一可知，目前一般的 OFDM 系統係以 DFT/IDFT 作為分頻的動作核心。這種架構的好處是硬體結構規律，而且已有快速演算法的硬體實現。然而如一些研究所指出[8]，分頻的動作也可以使用其他的運算代替，例如 SVD(奇值分解)或 DWT(離散小波轉換)。SVD 的運算量極大，且須隨通道變化而調整，故目前尚不實用。不過，隨著數位電路的飛速發展，也許在不久的將來確可考慮使用 SVD。

我們考慮以 SVD 實現 OFDM 的架構，並以模擬來評量其效能。結果證實，在相同的傳輸通道與傳輸訊雜比(SNR)，採用 SVD 的傳輸錯誤率比傳統的架構還小；參圖四。會得到這樣的結果最主要的原因是以 SVD 分頻後的次頻帶響應(subtone response)，其能量(absolute power)比起傳統的架構還高，這樣的現象在能量較低的次頻帶尤為明顯。因此，採用 SVD 的 OFDM 架構，可以有效的降低錯誤率，或者等效於降低傳輸能量(假定錯誤率和通道固定)。

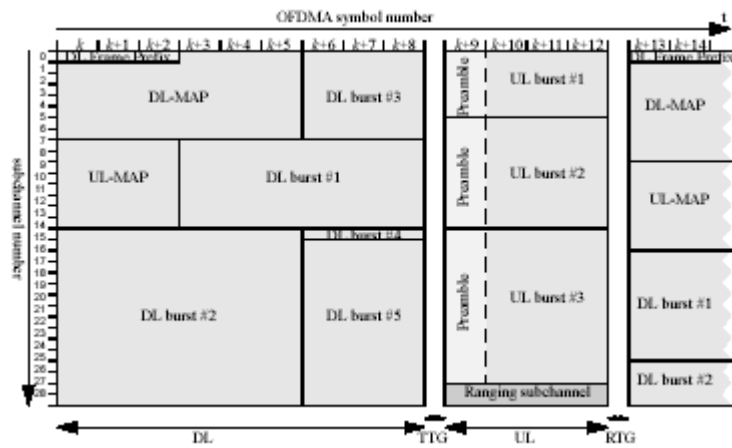
三、參考文獻

- [1] M.-T. Lin, “Fixed and mobile wireless communication based on IEEE 802.16a TDD OFDMA: transmission filtering and synchronization,” M.S. thesis, Dept. Electronics Engineering, National Chiao Tung University, June 2003.
- [2] Y.-P. E. Wang and R. Ramesh, “To bite or note to bite – a study of tail bits versus tail biting,” in *Proc. IEEE Int. Symp. Personal Indoor Mobile Radio Commun.*, vol. 2, pp. 317-321, Oct. 1996.
- [3] W. Sung and I.-K. Kim, “Performance of a fixed delay decoding scheme for tail biting convolutional codes,” in *IEEE Asilomar Conf. Signals Syst. Computers Conf Rec.*, vol. 1, pp. 704-708, Oct. 1996.
- [4] E. Zehavi, “8-PSK trellis codes for a Rayleigh channel,” *IEEE Trans. Commun.*, vol. 40, pp. 873-884, May 1992.
- [5] M. Speth, A. Senst, and H. Meyr, “Low complexity space-frequency MLSE for multi-user COFDM,” in *IEEE Global Telecommun. Conf. Rec.*, vol. 5, pp. 2395-2399, 1999.
- [6] F. Tosato and P. Bisaglia, “Simplified soft-output demapper for binary interleaved COFDM with application to HIPERLAN/2,” in *IEEE Int. Conf. Commun. Conf. Rec.*, vol. 2, pp. 664-668, 2002.
- [7] Y.-P. Ho, “Study on OFDM signal description and channel coding in the IEEE 802.16a TDD OFDMA wireless communication standard,” M.S. thesis, Dept. Electronics Engineering, National Chiao Tung University, June 2003.
- [8] A. Scaglione, G. B. Giannakis and S. Barbarossa, “Redundant filterbank precoders and equalizers. I. Unification and optimal designs,” *IEEE Trans. Signal Process.*, vol. 47, no. 2, pp. 1988–2006, July 1999.

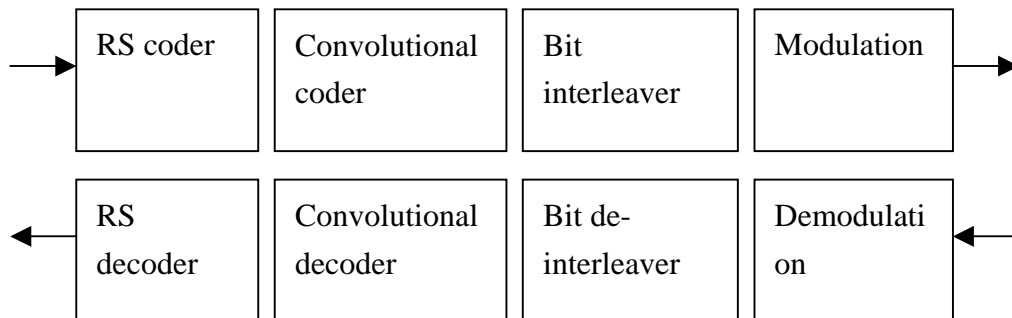
四、圖表



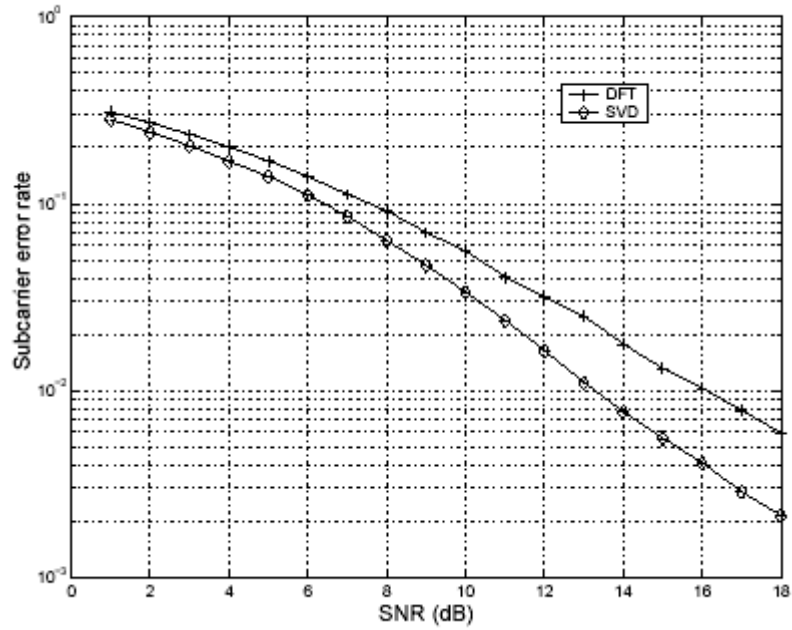
圖一：OFDMA 傳收系統簡圖



圖二：IEEE 802.16a OFDMA TDD 訊框架構(取自 802.16a 標準 Figure 128av)



圖三：IEEE 802.16a 之通道編解碼架構



圖四：使用 SVD 的系統與使用 DFT 的傳統 OFDM 傳輸錯誤率比較

Modulation	Uncoded Block Size (bytes)	Overall Coding Rate	Coded Block Size (bytes)	RS Code	CC Code Rate
QPSK	18	1/2	36	(24,18,3)	2/3
QPSK	26	~3/4	36	(30,26,2)	5/6
16-QAM	36	1/2	72	(48,36,6)	2/3
16-QAM	54	3/4	72	(60,54,3)	5/6
64-QAM	72	2/3	108	(81,72,4)	3/4
64-QAM	82	~3/4	108	(90,82,4)	5/6

表一：IEEE 802.16a 中六種不同的通道編碼組合(同 802.16a 標準 Table 116ce)

五、計畫成果自評

研究內容與原計畫相符程度：本子計畫為一個整合型計畫之一部分，本年度之研究達成了該整合型計畫之需求。

達成預期目標情況：本子計畫達成之貢獻形式，含創新之發現、理論之推導、技術水準之提昇、計算機模擬軟體之建立、人才培育。

成果之學術與應用價值等：本子計畫達成之科技領域成果，主要為對 IEEE 802.16a OFDMA 標準規範之了解、其 TDD 下鏈與上鏈時間與頻率同步方法之設計與模擬結果、其通道解碼方法之設計與模擬結果、以及對基於奇值分解之多載波調變效能研究。另亦考慮了適用之數位訊號處理實現平台，並對適用之無線通道模型及通道估計與等化方法作了初步研究。同步、通道解碼、與 SVD 多載波調變三方面之成果之學術價值高，我們正陸續撰寫論文投稿中。應用價值方面，所提出的同步方法與通道解碼方法，可為 IEEE 802.16a OFDMA 或相關傳收系統開發之參考。

綜合評估：本計畫獲得一些具有學術與應用價值的成果，並達人才培育之效。成效良好。

六、可供推廣之研發成果資料表

下頁起，共二頁。

可供推廣之研發成果資料表

可申請專利

可技術移轉

日期：92年8月26日

國科會補助計畫	計畫名稱：無線正交分頻多重進接頻道使用技術研究及全系統整合(I) 計畫主持人：林大衛 計畫編號：NSC 91-2219-E-009-008 學門領域：電信國家型計畫
技術/創作名稱	IEEE 802.16a OFDMA TDD 訊號同步方法
發明人/創作人	林孟亭、林大衛
技術說明	<p>中文：根據 IEEE 802.16a 標準中之 OFDMA TDD 規格設計的下鏈及上鏈傳輸之同步方法。其下鏈同步包括 OFDM symbol 之時間同步、頻率同步、及 TDD 訊框(frame)同步。上鏈同步則僅含時間同步，因為 802.16a 規格中對上鏈頻率誤差有限制，而訊框同步已於下鏈同步中達成。但不同用戶的上鏈 OFDM symbol 可有大至正負 25% 的 guard interval 長度的時間差，是使其時間同步複雜之一大因素。</p> <p>英文：Downlink (DL) and uplink (UL) synchronization methods designed according to the IEEE 802.16a standard's OFDMA TDD specifications. DL synchronization includes OFDM symbol time sync, frequency sync, and TDD frame sync. UL synchronization only includes time sync, for 802.16a specifies limit on UL frequency offset and frame sync is already achieved in DL sync. A major factor causing complexity in UL time sync is the allowed OFDM symbol time offset of up to plus-and-minus 25% of the guard interval length.</p>
可利用之產業及可開發之產品	無線通訊器材產業，IEEE 802.16a 或相關傳輸設備產品。
技術特點	根據 IEEE 802.16a 標準中之 OFDMA TDD 規格設計的下鏈及上鏈傳輸之同步方法。運算複雜度合理。
推廣及運用的價值	可用於 IEEE 802.16a 或相關傳輸設備產品。

1. 每項研發成果請填寫一式二份，一份隨成果報告送繳本會，一份送 貴單位研發成果推廣單位（如技術移轉中心）。
2. 本項研發成果若尚未申請專利，請勿揭露可申請專利之主要內容。
3. 本表若不敷使用，請自行影印使用。

可供推廣之研發成果資料表

可申請專利

可技術移轉

日期：92年8月26日

<p>國科會補助計畫</p>	<p>計畫名稱：無線正交分頻多重進接頻道使用技術研究及全系統整合(I) 計畫主持人：林大衛 計畫編號：NSC 91-2219-E-009-008 學門領域：電信國家型計畫</p>
<p>技術/創作名稱</p>	<p>IEEE 802.16a OFDMA 通道碼解碼方法</p>
<p>發明人/創作人</p>	<p>何玉屏、林大衛</p>
<p>技術說明</p>	<p>中文：根據 IEEE 802.16a 標準中之 OFDMA 規格設計的通道碼解碼方法，其中包括在位元間插(bit interleaving)與 QAM 調變之後的穿孔(punctured)去尾(tail-biting)迴旋碼之解碼法，及該標準特定之產生多項式(generator polynomial)下的縮短(shortened)里德-索羅門碼(RS code)之解碼法。以上迴旋碼係採軟式解碼，里德-所羅門碼則如一般做法，採硬式解碼。</p> <p>英文：Channel decoding method according to IEEE 802.16a standard's OFDMA specifications, including decoding of punctured tail-biting convolutional codes after bit interleaving and QAM modulation, and decoding of shortened Reed-Solomon (RS) code with 802.16a-specific generator polynomial. The convolutional decoder does soft-decision decoding whereas the RS decoder, as usual, does hard-decision decoding.</p>
<p>可利用之產業及可開發之產品</p>	<p>無線通訊器材產業，IEEE 802.16a 或相關傳輸設備產品。</p>
<p>技術特點</p>	<p>根據 IEEE 802.16a 標準中之 OFDMA 規格設計的通道碼解碼方法。其中迴旋碼解碼採軟式，而里德-所羅門碼解碼則為硬式。運算複雜度合理。</p>
<p>推廣及運用的價值</p>	<p>可用於 IEEE 802.16a 或相關傳輸設備產品。</p>

1. 每項研發成果請填寫一式二份，一份隨成果報告送繳本會，一份送 貴單位研發成果推廣單位（如技術移轉中心）。
2. 本項研發成果若尚未申請專利，請勿揭露可申請專利之主要內容。
3. 本表若不敷使用，請自行影印使用。

七、附錄

本附錄共含二篇會議論文初稿，如下列：

- A. M.-T. Lin and D. W. Lin, “Mobile wireless communication based on IEEE 802.16a TDD OFDMA: transmission filtering and synchronization” (6 pages).
- B. Y.-P. Ho and D. W. Lin, “Study on channel coding in the IEEE 802.16a OFDMA wireless communication standard” (6 pages).

Mobile Wireless Communication Based on IEEE 802.16a TDD OFDMA: Transmission Filtering and Synchronization

Meng-Ting Lin and David W. Lin

Department of Electronics Engineering and Center for Telecommunications Research
National Chiao Tung University
Hsinchu, Taiwan 30010, R.O.C.

E-mails: mtlin.ee90g@nctu.edu.tw, dwlin@mail.nctu.edu.tw

Abstract

We consider the use of IEEE 802.16a TDD (time-division duplex) OFDMA (orthogonal frequency division multiple access), originally developed for fixed wireless communication, for mobile communication. In particular, we consider the issues of transmission filtering and synchronization. For transmission filtering, in order to simulate multipath delays at non-integer sample spacing with ease, we design a four-times oversampled RRC (root-raised-cosine) filter that meets the power mask of the standard. For synchronization, we consider the DL (downlink) and the UL (uplink) separately. The designed DL synchronization method contains four stages. The first two use the guard interval to estimate the OFDM symbol start time and the fractional frequency offset, respectively. The third stage uses the guard bands and some pilot carriers to detect the integer frequency offset. And the final stage does frame synchronization using the information in the DL preamble. We consider two schemes for UL time synchronization by correlation of the received signal with the UL preamble. One does it in the time domain and the other in the frequency domain. Simulations are performed to investigate the performance.

1. Introduction

OFDM (orthogonal frequency division multiplexing) transmits data using a set of parallel low-bandwidth carriers. The carriers are independent of each other even though their spectra overlap, which results in bandwidth efficiency. High data rate systems are achieved by using a large number of carriers. OFDM symbols can be easily generated and received using inverse and forward fast Fourier transforms (IFFT and FFT), respectively. This technology has been used in several communication system standards.

To support multiple access, the carriers can be divided into subchannels. Each subchannel can have

This work was supported by the National Science Council of R.O.C. under grant no. NSC 91-2219-E-009-008.

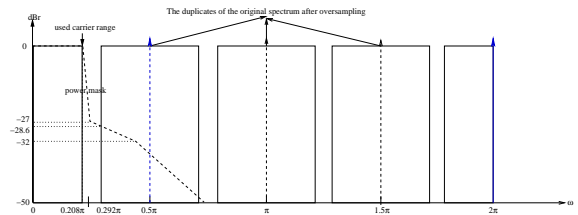


Fig. 1: Frequency spectrum of signal after four-times oversampling and its relation to the power mask.

multiple carriers that form one unit in frequency allocation, and different subchannels can be used by different users. This is OFDMA (orthogonal frequency division multiple access). In this work, we consider using the IEEE 802.16a WirelessMAN TDD OFDMA system [1], originally developed for fixed wireless communication, for mobile communication. In particular, we consider the issues of transmission filtering and synchronization. Proper transmission filtering is required to contain the emitted power spectrum and to limit intersymbol interference. And proper synchronization is required for good signal reception. We discuss these subjects in separate sections, followed by simulation results and a conclusion.

2. Transmission Filtering

In order to be able to simulate path delays at non-integer sample spacing, we consider four-times oversampled transmitter filtering employing a root-raised-cosine (RRC) filter. The output needs to meet the power mask specified in IEEE 802.16a as shown in Fig. 1.

The frequencies from 0.208π to 0.292π in Fig. 1 correspond to the guard bands, and therefore the RRC filter need not be concerned about this part. Thus the critical point in filter design is the lowest frequency of the first duplicate (0.292π). The filter needs to have a smaller value than the power mask at this frequency. After some computation, we find that a 57-tap RRC

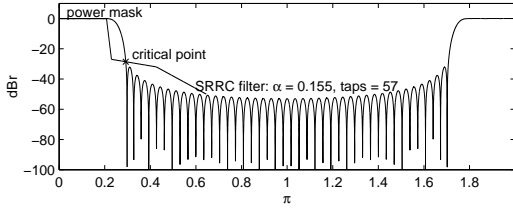


Fig. 2: Frequency spectrum of 57-tap RRC filter with roll-off factor = 0.155.

filter with $\alpha = 0.155$ can comply with the power mask requirement, as shown in Fig. 2. We consider using the same design for matched-filtering in the receiver.

As the aliasing would be small after four-times downsampling over the filtered received signal, we can apply downsampling before synchronization to reduce the receiver complexity. The length of the combined impulse response of a 57-tap transmitter filter and a 57-tap receiver filter is 29 nonoversampled samples. To account for non-integer-delay channel multipaths and possible sampling phase errors, therefore, the guard interval in the OFDM symbol that could be used to deal with multipath delays is reduced by 28 samples.

For efficiency in computation, polyphase decomposition can be employed in both the transmitter filter and the receiver filter.

3. Synchronization

Accurate demodulation and detection of an OFDM signal requires carrier orthogonality. Variations of the carrier oscillator, sample clock or the symbol time affect the orthogonality and the system performance. In this study, the sample clocks of the user station and the base station are assumed to be identical. Hence we only consider timing and frequency synchronization.

3.1. Some IEEE 802.16a Specifications

The carriers are divided into three types: data, pilot, and null (guard bands and DC carrier) which transmit nothing at all. Table 1 shows the specifications. The pilot carriers in DL (downlink) transmission are partitioned into fixed-location and variable-location pilots. The carrier indices of the fixed-location pilots never change. The variable-location pilots shift their locations every symbol depending on the value of L (L cycles through 0, 2, 1, 3) periodically every 4 symbols. The PRBS generator is used to produce a sequence, w_k , where k corresponds to the carrier index. The value of the pilot modulation on carrier k is then derived from w_k . The initialization vector of the PRBS in DL transmission is [1111111111] except for the OFDMA DL PHY preamble. For the UL (uplink), the initialization vector is [1010101010].

Table 1: OFDMA Carrier Allocations

Parameter	DL Value	UL Value
Total number of carriers	2048	2048
Number of DC carriers	1	1
Number of guard carriers, left	173	176
Number of guard carriers, right	172	175
Total number of pilots	166	160
Number of data carriers	1536	1536
N_{used} , number of used carriers (data carriers + pilot carriers)	1702	1696

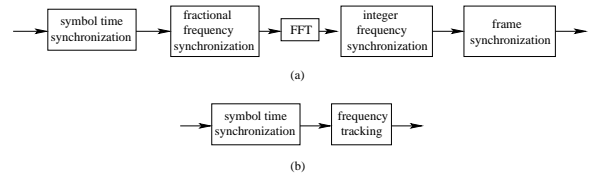


Fig. 3: Method of synchronization. (a) Initial synchronization. (b) Normal synchronization.

The pilots of the first three OFDM symbols is the DL preamble in the sense that they indicate where the OFDMA frame starts. UL preamble is the first symbol of the UL transmission and all used carriers in this symbol are pilots. For the DL preamble, the initialization vector of the pilot modulation PRBS is [010101010]. Hence the preamble and other symbols may have the same pilot locations, but they can be recognized by different modulation values.

3.2. Downlink Synchronization

There are two DL synchronization conditions: initial synchronization and normal synchronization. If a subscriber wants to join the transmission network for the first time, both time and frequency need be synchronized. In our design, the initial DL synchronization is divided into 4 stages, as shown in Fig. 3(a). For normal synchronization, the frame (symbol) start time is already known roughly and the frequency has been synchronized. As a result, only two stages are needed to detect the symbol start time and to track the frequency offset, as shown in Fig. 3(b). Here we only focus on the initial synchronization.

The first two stages of DL initial synchronization is based on the algorithm in [3] and [4] that employ the maximum likelihood approach to estimate time and frequency offsets. Under the assumption that the received samples are jointly Gaussian, symbol time offset $\hat{\theta}$ and fractional frequency offset $\hat{\epsilon}$ are given by

$$\hat{\theta} = \underset{\theta}{\operatorname{argmax}} \{ |\Gamma(\theta)| - \rho \Phi(\theta) \} \quad (1)$$

and

$$\hat{\epsilon} = \frac{-1}{2\pi} \angle \Gamma(\hat{\theta}), \quad (2)$$

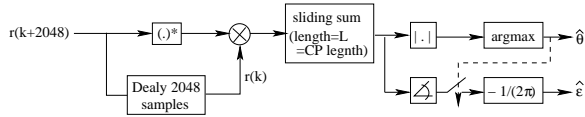


Fig. 4: The structure of the symbol time and frequency estimator.

where

$$\Gamma(\theta) = \sum_{k=\theta}^{\theta+L-1} r(k)r^*(k+N), \quad (3)$$

$$\Phi(\theta) = \frac{1}{2} \sum_{k=\theta}^{\theta+L-1} |r(k)|^2 + |r(k+N)|^2, \quad (4)$$

and $\rho = \frac{SNR}{SNR+1}$ with SNR being signal to noise ratio.

The symbol time offset estimator can be viewed as consisting of two parts: the correlation $\Gamma(\theta)$ that correlates the received sampled baseband signal, r , with a delayed version of itself, and a part that compensates for the difference in energy in the correlated samples. We drop the second part to reduce the complexity. The structure of this new estimator (guard interval correlator) is shown in Fig. 4.

The third stage uses the guard bands and two pilot carriers (the edges of used carriers) to detect the integer frequency offset. The first step is to determine the received OFDM symbol is transmitted from the BS (DL) or other SSs (UL). The number of the UL guard carriers is larger than DL by 6 carriers. A threshold can be set and if any of these 6 carriers is larger than the threshold, the SS will regard the received symbol as the DL symbol.

If there is no integer frequency offset, the FFT outputs of all the guard carriers will be small. So, all the guard carriers are checked to see if any of them exceeds the threshold. The checking direction is from higher frequency to lower frequency. If the carrier is detected to be larger than the threshold in the checking procedure, the check is stopped and the frequency is corrected. The check and correction take turns until all the guard carriers are checked to be smaller than the threshold. An additional check is added to see whether both edges of the used carriers (pilot carriers) are larger than the threshold. After these three checks, the integer synchronization finishes. The threshold is chosen to be 0.55 in our simulation.

The fourth stage use the DL preamble to determine when a new frame starts. The same as stage III, the SS has to check whether the received signal is from the BS. Then, for a DL symbol, it is required to check whether the symbol is the beginning of a frame. The SS knows the values of DL preamble and pilots, so it can use them as the reference data, as shown in Table 2. The FFT outputs are correlated with these 7 possible cases of the reference data. If the received symbol has the same pilot locations and the same initial vector of

Table 2: 7 Cases of Reference Information in Frame Synchronization

DL preamble (L , PRBS)	DL normal symbol (L , PRBS)
0, 01010101010	0, 11111111111
1, 01010101010	2, 11111111111
2, 01010101010	1, 11111111111
	3, 11111111111

modulation PRBS with the reference data, the correlation of them will be larger than the other 6 cases. A frame is determined to start if there are three successive DL symbols with the maximum correlation corresponding to the preamble.

However, the performance of this method goes down significantly when the time synchronization in stage I does not detect the correct location. To solve this problem, we apply the FFT for the region from -32 to 32 samples in offset with the detected symbol start location in stage I. In order to reduce the complexity of FFT, the conventional FFT is only applied to the location -32 . When a new data value is received, the simplified FFT below is used:

$$X_n(k) = [X_{n-1}(k) - x_{n-N} + x_n] e^{j\frac{2\pi k}{N}}, \quad (5)$$

where N is the FFT size, k is the carrier index, n is sample number, and x_n is the new incoming sample. After observing the correlation for 65 sample times, the location with peak correlation is assumed to be the real symbol start time. The maximum correlation of 7 cases is robust enough to be used.

3.3. Uplink Synchronization

Assuming a successful initial synchronization and ranging, the mobile enters the time and frequency grid with a low offset in time and frequency. No frequency synchronization is done in UL normal transmission. What the BS has to do is to detect the exact UL symbol arrival time. According to 802.16a, the SSs shall acquire and adjust their timing such that all uplink OFDM symbols arrival times coincident at the BS to an accuracy of $\pm 25\%$ of the minimum guard-interval or better. The BS shall detect the arrival time of the first coming signal to keep the symbol ISI free.

Two UL synchronization schemes are considered. One is using the correlation of the preamble in the frequency domain and the other is in the time domain. There are two stages in both schemes. The first stage uses the timing part of the joint ML estimator to detect roughly the symbol start time. The actual arrival time of the first arriving signal is likely before the detected time. As the user arriving time may vary as much as 50% of the guard interval, we apply the preamble correlation for the samples up to 50% of the guard interval earlier than the detected symbol start time. Figure 5 shows the UL synchronization stage II by frequency domain approach. The FFT outputs are corre-

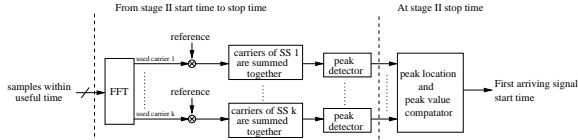


Fig. 5: Illustration of UL stage II by frequency domain approach.

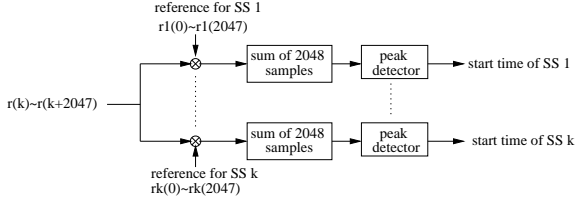


Fig. 6: Illustration of UL stage II by time domain approach.

lated with the preamble reference values over all the subchannels used by each SS. For time domain approach, the received samples are correlated with reference data string which is the IFFT output according to the subchannels used by each SS. The UL synchronization stage II by time domain approach is shown in Fig. 6.

4. Simulation Results

4.1. Downlink Synchronization

Table 3 specifies the transmission parameters of our simulation system based on IEEE 802.16a. We applied three channel environments in simulation of DL stage I and II: AWGN channel, one-path Rayleigh fading channel and multipath Rayleigh fading channel. The used multipath channel model is chosen from one of the channel environments defined by ETSI, as shown in Table 4 [2]. The SNR of additive noise is assumed to be 10 dB in the fading channels. As for the last two DL synchronization stages, the simulation is taken in the multipath channel. Note that the velocity 60 km/hr would result in the maximum Doppler shift $f_d T_s = 0.112$ (333 Hz) in our simulation condition.

We have simulated the DL stage I, time synchronization, by using time part of the ML estimator and

Table 3: System Parameters Used in Simulation

Number of carriers	2048
Center frequency	6 GHz
Uplink / Downlink bandwidth	6 MHz/ 6 MHz
Carrier spacing (Δf)	3.348 kHz
Sampling frequency (f_s)	6.86 MHz
OFDM symbol time (T_s)	336 μ sec
Useful time (T_b)	298 $\frac{2}{3}$ μ sec (2048 samples)
Cyclic prefix time (T_g)	37 $\frac{1}{3}$ μ sec ($\frac{1}{8} T_b = 256$ samples)

Table 4: Channel Impulse Response Model of ETSI “Vehicular A” Channel Environment

tap	relative delay (nsec)	average power (dB)
1	0	0
2	310	-1.0
3	710	-9.0
4	1090	-10.0
5	1730	-15.0
6	2510	-20.0

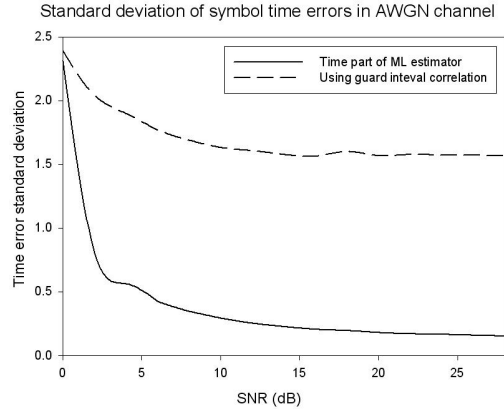


Fig. 7: Standard deviations of time offset estimation errors in AWGN channel by using ML estimator and guard interval correlator (stage I).

guard interval correlation. Figure 7 shows the standard deviation of these two methods. The standard deviation is a measure of how spread out a distribution is, and is defined as $\sqrt{E \left\{ \left| \theta - \hat{\theta} \right|^2 \right\}}$. The ML estimator has better performance than the guard interval correlator in the AWGN channel. However, from Fig. 8, we can find that the guard interval correlator performs better in the fast fading channel. So we can use the guard interval correlator in the fading channel to reduce the complexity. Note that the time synchronization performance in one path channel is worse than multipath channel when the Doppler shift is not zero. The channel variation causing by Doppler spread destroys the autocorrelation property. However, the multipath channel in some sense provides the time diversity. For all paths, the fading conditions are different so that the autocorrelation property would be stronger than one path environment.

The added frequency offset to simulate fractional frequency synchronization (stage II) is 0.1 carrier spacings. The standard deviation is defined by $\sqrt{E \left\{ \left| \epsilon - \hat{\epsilon} \right|^2 \right\}}$. The performance has no difference by using two DL stage I schemes. The reason is that the value of the frequency estimation is almost the same for a small nearby range of the symbol start location. Thus we can know that this estimator is ro-

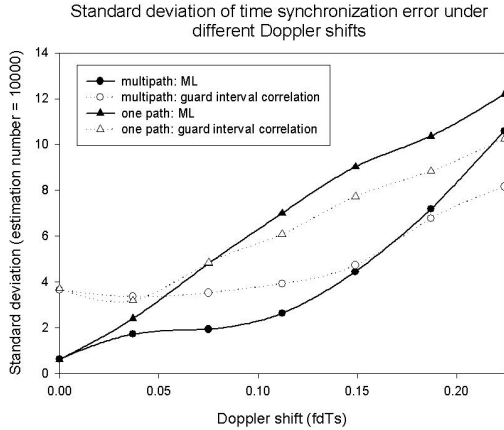


Fig. 8: Standard deviations of time offset estimation errors in one path channel and multipath channel by using ML estimator and guard interval correlator (stage I).

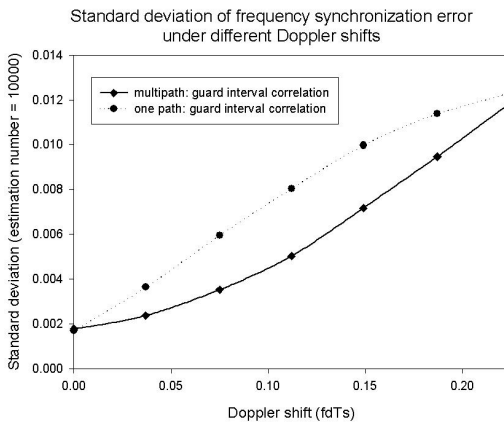


Fig. 9: Performance of DL fractional frequency offset synchronization in one-path and multipath Rayleigh fading channels (stage II).

bust. Figure 9 compares the frequency synchronization performance under one-path and multipath fading channels. The fractional frequency synchronization utilize the autocorrelation property of the OFDM symbol. The one-path channel destroys this property more seriously than multipath channel, so the performance is better in multipath channel.

Table 5 shows the failure probability of the integer frequency synchronization (stage III) and the required DL symbol number to finish the synchronization from stage I to stage III. The needed time to sync the signal tends to be longer as the Doppler shift becomes larger. The integer frequency synchronization can correct the offset from -173 to 172 carrier spacings which is about -579 KHz to 576 KHz in this simulation.

The frame synchronization (stage IV) error probability is shown in Table 6. Note that IEEE 802.16a is designed for the fixed environments. Observing

Table 5: Performance of DL Integer Frequency Synchronization (Stage III) at Different Maximum Doppler Shifts

Doppler shift $f_d T_s$	Integer synchronization failure probability estimation frames: 5000	Average required symbol delay to complete integer frequency synchronization
0	0.26 %	8.90
0.037	0.11 %	12.67
0.075	0 %	12.02
0.112	0 %	11.85
0.149	0.08 %	12.02
0.187	0.32 %	12.34
0.224	1.22 %	14.15

Table 6: Performance of DL Frame Synchronization (Stage IV) at Different Maximum Doppler Shifts

Doppler shift $f_d T_s$	Frame synchronization false alarm probability estimation frames: 5000	Average required frame delay to complete frame synchronization
0	0 %	1.69
0.037	0 %	2.1
0.075	0 %	2.06
0.112	0.004 %	2.18
0.149	0.004 %	2.24
0.187	0.019 %	2.37
0.224	0.01 %	2.6

the simulation result, the useable information is really enough when the Doppler spread is small. But when the Doppler spread is large, we may need a better DL preamble format or additional MAC layer information to check the received signal after demodulation.

4.2. Uplink Synchronization

We simulate the case with 3 SSs. UL burst1 is transmitted by SS1 using 8 subchannels. UL burst2 is transmitted by SS2 using 16 subchannels. UL burst3 is transmitted by SS3 using 8 subchannels. The arriving times of burst1 and burst2 differ by 25% of the guard interval, which is 64 sample time, while burst3 lags burst1 by 50% of the guard interval, which is 128 sample time. We only apply the multipath fading channel to simulate the UL synchronization.

The time offset standard deviations for both UL synchronization schemes are shown in Fig. 10. If there is no Doppler shift, we can always detect the correct symbol start time of the first coming signal by both approaches. When the Doppler shift is not zero, the performance of frequency domain approach is decreased as the Doppler spread increases. As for the time domain approach, the Doppler shift has no obvious effects on the synchronization performance except when it is very small.

The top plot in Fig. 11 represents the multipath channel model that is specified in non-oversampling sample numbers and with average power in normal scale. The synchronization error distributions for the signals from three different SSs are compared together with the channel model in the bottom plot of Fig. 11. Comparing the time error distribution with the channel

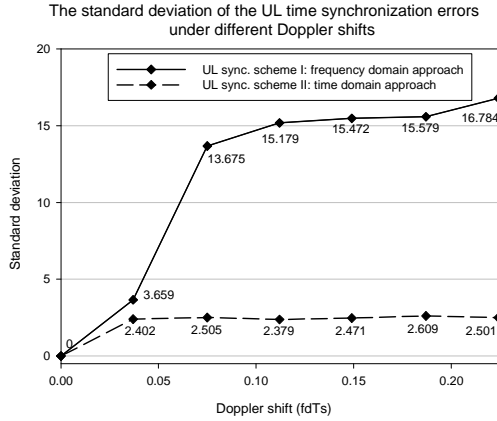


Fig. 10: Standard deviation of UL symbol time synchronization errors by using frequency and time domain approaches.

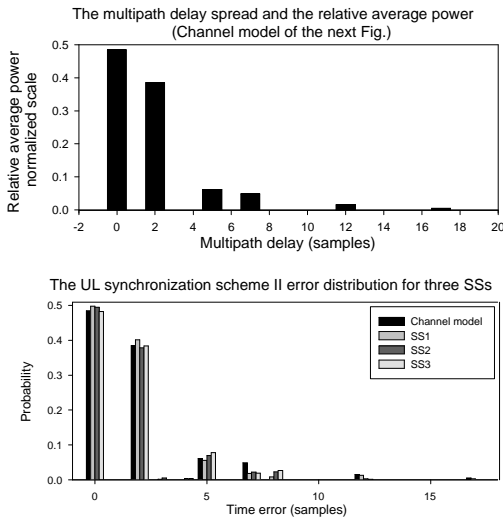


Fig. 11: Performance of UL time synchronization scheme II: errors of three signal with different arriving times, under different Doppler spreads.

model, we see that the different time offsets obtained at synchronizer output almost concur with the sample number of the multipath delays. Furthermore, the occurrence probabilities at the different time offsets are proportional to the relative average power of the paths. No matter when the signal arrives, the synchronization performance has no difference. Thus we can roughly detect the start time of all signals from different SSs and this information should be helpful for channel estimation.

5. Conclusion and Future Work

In order to simulate non-integer multipath delays, we have applied 4-times oversampling to the transmitted

signal. By the specification of the transmit spectral mask in 802.16a, a 57-taps RRC filter with roll-off factor 0.155 is designed to suppress the out-of-band power.

We have designed the synchronization schemes for DL and UL receivers and analysed the performance under AWGN and fading channels. For DL, the time and fractional frequency synchronization would work well in the AWGN channel and the fading channel with the Doppler shift lower than $0.1f_dT_s$. The integer frequency synchronization ability to correct frequency offset is from -173 to 172 carrier spacings and the error probability were about 10^{-4} to 10^{-2} in the multipath fading channel. Frame synchronization is always correct when the Doppler shift was smaller than $0.08f_dT_s$. In summary, the DL synchronization scheme was suitable for the environment that the maximum Doppler shift was smaller than $0.1f_dT_s$.

As for UL, the correlation in the time domain has better performance. The time synchronization errors are in some degree correlated to the channel model. Thus the guard interval should be at least larger than two times of the delay spread.

There are several possible extensions for our research. The synchronization performance can be analyzed for different guard interval lengths. We can try to do DL frame synchronization by using the correlation in the time domain. Further, the simulation so far has been done using floating-point arithmetic. If hardware implementation is in view, then fixed-point simulation should be considered for implementation efficiency.

6. References

- [1] IEEE Std 802.16a-2003, *IEEE Standard for Local and Metropolitan Area Networks — Part 16: Air Interface for Fixed Broadband Wireless Access Systems — Amendment 2: Medium Access Control Modifications and Additional Physical Layer Specifications for 2–11GHz*. New York: IEEE, April 1, 2003.
- [2] M. Goldhammer *et al.*, “OFDM (FFT 256) fixed and mobile system considerations,” *IEEE 802.16e contribution* – 03/07.
- [3] J. J. van de Beek, *et al.*, “ML estimation of time and frequency offset in OFDM systems,” *IEEE Trans. Signal Processing*, vol. 45, no. 7, pp. 1800–1805, July 1997.
- [4] J. J. van de Beek, P. O. Borjesson, M. L. Boucheret, D. Landstrom, J. M. Arenas, P. Odling, C. Ostberg, M. Wahlqvist, and S. K. Wilson, “A time and frequency synchronization scheme for multiuser OFDM,” *IEEE J. Select. Areas Commun.*, vol. 17, pp. 1900–1914, Nov. 1999.

STUDY ON CHANNEL CODING IN THE IEEE802.16A OFDMA WIRELESS COMMUNICATION STANDARD

Yu-Ping Ho and David W. Lin

Dept. of Electronics Engineering and Center for Telecommunications Research
National Chiao Tung University
Hsinchu, Taiwan 30010, R.O.C.
E-mails: u860913@micro.ee.nthu.edu.tw, dwlin@mail.nctu.edu.tw

ABSTRACT

IEEE802.16a employs concatenated coding with Reed-Solomon (RS) outer code and convolutional (CC) inner code, followed by bit interleaving before M -ary QAM modulation. The RS code is shortened and punctured, and the CC code is punctured and of the tail-biting type. In this paper, we consider the code properties, their decoding, and the associated decoding performance. For the tail-biting punctured CC codes, we propose a low-complexity decoder. It turns out that the bit interleaver and the M -QAM modulation impact the design and the performance of the CC decoder significantly. We simulate the RS codes, the CC codes, and the concatenated codes respectively in AWGN channel, and compare the simulation results with theoretic coding gains calculated based on minimum codeword distances. We find that the performance of the RS codes and the CC codes almost achieves the theoretic values, which means that our decoders have good performance. The performance of the concatenated codes is worse at the E_b/N_0 considered. We conjecture that their performance will also approach the theoretic values at high E_b/N_0 .

1. INTRODUCTION

In the wireless channel, channel coding is an important technique to reduce the bit error rate. The channel coding scheme used in IEEE802.16a [1], as shown in Fig. 1, is a concatenated code employing the Reed-Solomon (RS) code as outer code and convolutional (CC) code as inner code. Input data streams are divided into RS blocks, then each RS block is encoded by a tail-biting CC code, which can be viewed as a block code and hence makes the whole concatenated code a block-based coding scheme. In addition, between the CC coder and the modulator is a bit interleaver, which protects the CC code from severe impact of burst errors and increases overall coding performance. This approach has

This work was supported by the National Science Council of R.O.C. under grant no. NSC 91-2219-E-009-008.

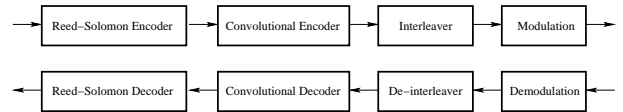


Fig. 1: Channel coding structure.

been termed “bit-interleaver coded modulation (BICM)” in the literature [6]. The bit interleaver greatly complicates the branch metric for soft-decision CC decoding via the Viterbi algorithm.

To make the system more flexibly adaptable to the channel condition, there are six coding-modulation schemes defined in IEEE 802.16a, as shown in Table 1. The different coding rates are made by shortening and puncturing of the native RS code through one RS coder and with puncturing of the native tail-biting CC code through one CC coder.

The organization of this paper is as follows: Section 2 analyzes coding gains of the six coding-modulation schemes based on minimum codeword distance. Section 3 designs decoders for the shortened and punctured RS code, tail-biting punctured CC code, and BICM. Section 4 compares the performance of the decoders we design with the analytic coding gains. Section 5 is our conclusion.

2. CODING GAIN ANALYSIS BASED ON MINIMUM CODEWORD DISTANCE

2.1. Reed-Solomon Coding Gain

A crude estimate of a T -error correcting RS coding gain with soft-decision in AWGN is

$$10 \log_{10}(R_c \cdot d_{min}) \text{ dB}, \tag{1}$$

where R_c is the code rate [9]. But since RS codes are usually hard-decision decoded, the coding gains are reduced by $\frac{2T+1}{T+1}$ dB [12]. The results are listed in Table 2.

Table 1: Six Channel Coding Schemes

Scheme	Modulation	Overall Code Rate	RS Code	CC Code Rate	CC Code d_{free}
1	QPSK	1/2	(24, 18, 3)	2/3	6
2	QPSK	$\sim 3/4$	(30, 26, 2)	5/6	4
3	16QAM	1/2	(48, 36, 6)	2/3	6
4	16QAM	3/4	(60, 54, 3)	5/6	4
5	64QAM	2/3	(81, 72, 4)	3/4	5
6	64QAM	$\sim 3/4$	(90, 82, 4)	5/6	4

Table 2: Coding Gain Based on Minimum Codeword Distance

Scheme	Hard-Decision RS Coding Gain (dB)	Soft-Decision CC Coding Gain (dB)	Concatenated Coding Gain (dB)
1	4.77	6.02	10.79
2	4.15	5.23	9.38
3	7.2	6.02	13.22
4	5.56	5.23	10.79
5	6.48	5.74	12.22
6	6.59	5.23	11.82

2.2. Convolutional Coding Gain

A rough estimate of soft-decision CC coding gain in AWGN is

$$10 \log_{10}(R_c \cdot d_{free}) \text{ dB}, \quad (2)$$

where R_c is the code rate and d_{free} is the free distance [9]. The results are listed in Table 2.

2.3. Concatenated Coding Gain

The theoretic concatenated coding gain is the product of the coding gain of the outer code and the inner code. It is a very loose upper-bound for most concatenated codes, except in the case of turbo codes. The results are listed in Table 2.

3. DECODER DESIGN

3.1. Shortened and Punctured Reed-Solomon Code

The Reed-Solomon code in IEEE802.16a is derived from a systematic RS ($N = 255$, $K = 239$, $T = 8$) code on $GF(2^8)$, where N is number of overall bytes after encoding,

K is number of data bytes before encoding, and T is number of data bytes which can be corrected. The field generator polynomial is $p(x) = x^8 + x^4 + x^3 + x^2 + 1$. The generator polynomial for RS code can be generalized as

$$g(x) = (x + \lambda^h)(x + \lambda^{h+1}) \dots (x + \lambda^{h+2T-1}), \quad (3)$$

where h can be any integer. Usually, $h = 1$. However, for the RS code in IEEE802.16a $h = 0$. This affects the decoding algorithm, as shown later.

This code then is shortened and punctured to enable variable block sizes and variable error-correction capability. The modified RS code is denoted as (N', K', T') , listed in the Table 1. They are shortened to K' data bytes and punctured to permit T' bytes to be corrected. When a block is shortened to K' data bytes, the first $239 - K'$ bytes of the encoder input blocks are zeros. When a codeword is punctured to permit T' bytes to be corrected, only the first $2T'$ of the total 16 parity bytes are employed.

The Euclid's algorithm is a common (hard-decision) decoding algorithm for RS codes [10]. It includes four steps:

1. Compute the syndrome value.
2. Compute the error location polynomial.
3. Compute the error location.
4. Compute the error value.

The shortening does not affect the RS decoder because the RS code in IEEE802.16a is a systematic code and the initial zero bytes will not affect each step of the decoder. As for the puncturing, the punctured bytes can be viewed as erasures.

By the use of $h = 0$ in IEEE802.16a, step 1 and 4 of the decoding algorithm need to be modified [11]. To see how, note that the syndrome value computed in step 1 is S_h for the root of $x = \lambda^h$, S_{h+1} for the root of $x = \lambda^{h+1}$, \dots , and S_{h+2T-1} for the root of $x = \lambda^{h+2T-1}$. The error value computed in step 4 for any h is the error value computed for $h = 1$ multiplied by $x_k^{-(h-1)}$, where k denotes the error location. Since $h = 0$ for the RS code in IEEE802.16a, the syndrome value is $S_0, S_1, \dots, S_{2T-1}$ and the error value is the error value computed for $h = 1$ multiplied by x_k^1 .

3.2. Tail-Biting Punctured Convolutional Code

Each RS block is encoded by a binary convolutional encoder, which has native rate of 1/2, a constraint length equal to 7, and the generator polynomials for the two output bits are 171_{OCT} and 133_{OCT} .

This CC code is then punctured to allow different rates. Furthermore, tail-biting is performed, by initializing the encoder's memory with the last data bits of the RS block. Puncturing does not affect the Viterbi decoding algorithm

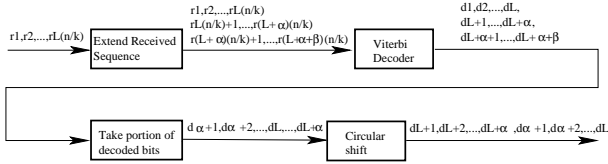


Fig. 2: Tail-biting convolutional decoder.

very significantly. The metrics associated with the punctured bits are simply disregarded in metric accumulation [2].

IEEE802.16a uses the tail-biting approach, which has better performance compare with direct-truncation CC code and does not lose rate compared with zero-tail CC code. However, we pay the cost of a complex decoder. The optimal decoder of tail-biting CC code, as suggested in [3], is to run 2^m (m is register length, and m is 6 here.) parallel Viterbi decoders, each decoder postulating a different starting and ending state. The Viterbi decoder that produces the globally best metric gives the maximum likelihood estimate of the transmitted bits. The obvious disadvantage of this method is the 2^m times complexity compared to decoding for the code with tail bits. Therefore, combined [4] and [5], we propose a suboptimal decoder which can reduce the complexity to less than 2 times the normal Viterbi algorithm. The performance is shown in Section 4.

Our suboptimal tail-biting CC decoder is depicted in Fig. 2. We first extend the received sequence by repeating the first $(\alpha + \beta)(n/k)$ received bits, where α and β are two important parameters that we have to set. In the Viterbi decoder, the trellis is initialized by making all states equally likely (i.e., setting the a priori probabilities of all survivors equal), and the Viterbi algorithm is executed for the extended received sequence. A traceback is performed from the best state at the end of the extended received sequence, and a portion of the data in the decoded block, from position α on for the length of information bits, is chosen as the estimate of the data block.

This scheme relies on the fact that if the received sequence is circularly repeated, the trellis of the extended received sequence can be considered circular since tail-biting code starts and ends in the same state. The trellis of the tail-biting CC decoder is depicted in Fig. 3. Because the starting state is unknown, the first α surviving paths of the decoder may not be the correct paths. Only after enough depth can the surviving paths approach the correct ones. Thus the later part of the decoded block will be more like to the information data.

Furthermore, we need to consider the traceback mechanism. The surviving path will be almost unique after some depth into the trellis. Therefore, the trellis can be truncated and the traceback mechanism performs after some delay, say τ . The conventional value of τ is 5 times the register

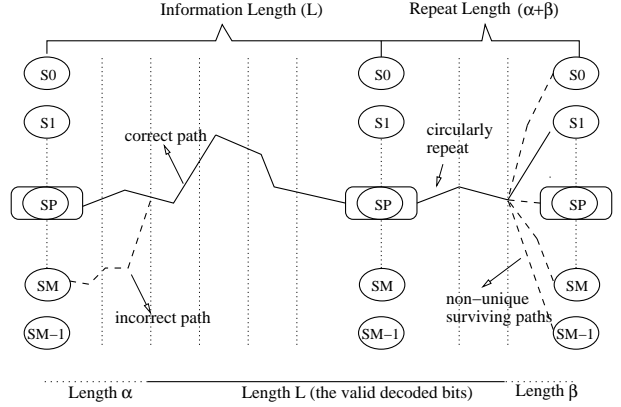


Fig. 3: Trellis of tail-biting convolutional code.

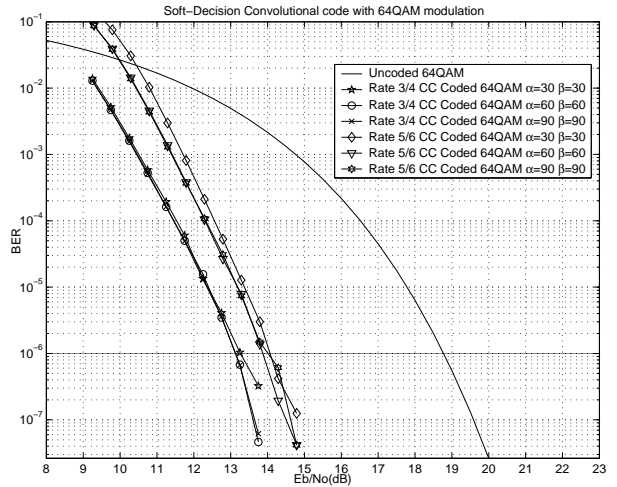


Fig. 4: Soft-decision CC decoding performance in AWGN with $\alpha = \beta = 30, 60,$ and 90 of the six coding schemes.

length [2]. Since the ending state of the trellis for the extended received data is unknown and the decision depths for the latest decoded data are not long enough to make the surviving paths unique, the latest decoded data will not be reliable and can't be chosen as the decoded data. The unreliable data length is set to β , which is related (actually equal) to τ .

To decide the values of α and β , we run simulation under different E_b/N_0 for $\alpha = \beta = 30$, $\alpha = \beta = 60$, and $\alpha = \beta = 90$ for the six coding schemes in AWGN. We show simulation results of scheme 5 and 6 in Fig. 4; other schemes have similar simulation results. We find the performance is almost the same for $\alpha = \beta = 60$ and $\alpha = \beta = 90$, and both are better than $\alpha = \beta = 30$. Considering the trade-off between performance and decoder complexity, we adopt $\alpha = 60$ and $\beta = 60$ in the Viterbi decoder.

3.3. Bit-Interleaved Coded Modulation Code

For optimal soft-decision Viterbi decoding in AWGN channel, the metric is the Euclidean distance between each trellis path and the soft-output of the demodulator. The problem now is that there is a bit interleaver between the CC encoder and the modulator in the transmitter. Thus, we adopt a suboptimal decoder based on bit-by-bit metric computation, which is proposed in [6], [7], and [8].

Let $a[i] = a_I[i] + ja_Q[i]$ denote the QAM symbol transmitted in the i th sub-carrier of OFDM symbol and $\{b_{I,1}, \dots, b_{I,k}, \dots, b_{I,t}, b_{Q,1}, \dots, b_{Q,k}, \dots, b_{Q,t}\}$ be the corresponding bit sequence. Assuming that the ISI (inter OFDM symbol interference) and ICI (inter channel interference) are completely eliminated, then the received signal of the sub-carrier can be written as

$$r[i] = G_{ch}[i] \cdot a[i] + w[i], \quad (4)$$

where $G_{ch}[i]$ is the channel frequency response complex coefficient for the i th sub-carrier and $w[i]$ is the complex Additive White Gaussian Noise (AWGN) with variance $\sigma^2 = N_0$. If the channel estimate is error free, the output of the one-tap equalizer is given by

$$y[i] = a[i] + w[i]/G_{ch}[i] = a[i] + w'[i], \quad (5)$$

where $w'[i]$ is still complex AWGN noise with variance $\sigma'^2(i) = \sigma^2/|G_{ch}[i]|^2$.

Assuming that $G_{ch}[i]$ is known to the receiver and that the transmitted bits are i.i.d, the following maximization is performed to estimate the encoded bit sequence \mathbf{b} according to the ML (maximum likelihood) criterion:

$$\hat{\mathbf{b}} = \arg \max_{\mathbf{b}} P[\mathbf{r}|\mathbf{b}]. \quad (6)$$

For each in-phase($b_{I,k}$) and quadrature($b_{Q,k}$) bit, two metrics are derived corresponding to the two possible values 0 and 1, respectively. For bit $b_{I,k}$, first the QAM constellation is split into two partitions of complex symbols, namely $S_{I,k}^{(0)}$ comprising the symbols with a "0" in position (I, k) and $S_{I,k}^{(1)}$, which is complementary. Then the two metrics are obtained by

$$\begin{aligned} m'_c(b_{I,k}) &= \sum_{\alpha \in S_{I,k}^{(c)}} \log p(r[i]|a[i] = \alpha) \\ &\approx \max_{\alpha \in S_{I,k}^{(c)}} \log p(r[i]|a[i] = \alpha), \quad c = 0, 1(7) \end{aligned}$$

Since the conditional pdf of $r[i]$ is complex Gaussian

$$p(r[i]|a[i] = \alpha) = \frac{1}{\sqrt{2\pi\sigma}} \exp\left\{-\frac{1}{2} \frac{|r[i] - G_{ch}[i]\alpha|^2}{\sigma^2}\right\}, \quad (8)$$

Table 3: Bit Metric for Method-ML and Method-LLR

	Method-ML	Method-LLR
Bit metric (decided "0")	m_0	$[\frac{1}{4}(m_0 - m_1) + 1]^2$
Bit metric (decided "1")	m_1	$[\frac{1}{4}(m_0 - m_1) - 1]^2$

and $r[i] = G_{ch}[i] \cdot y[i]$, the metrics defined in Eq. (7) are equivalent to

$$m_c(b_{I,k}) = |G_{ch}[i]|^2 \cdot \min_{\alpha \in S_{I,k}^{(c)}} |y[i] - \alpha|^2. \quad (9)$$

Finally, these metrics are de-interleaved, i.e., each couple (m_0, m_1) is assigned to the bit position in the decoded sequence according to the de-interleaver map, and fed to the Viterbi decoder which selects the binary sequence with the smallest cumulative sum of metrics. We name this method *Method-ML* in the following discussion.

From the concept of Log-Likelihood Ratio (LLR), a method named *Method-LLR* is proposed in [8]. Because of the Gray-coding used in the M -ary QAM constellation, this method can reduce the complexity of *Method-ML*. It defines $LLR(b_{I,k})$ as follows (the following applies to the quadrature part, too).

$$\begin{aligned} LLR(b_{I,k}) &= (m_0(b_{I,k}) - m_1(b_{I,k}))/4 \\ &= |G_{ch}[i]|^2 \cdot D_{I,k}. \end{aligned} \quad (10)$$

The metrics sent to the Viterbi decoder of the two methods are defined in Table 3. Note that the difference between the bit metrics for the decided "0" and "1" is the same for the two methods, namely $\pm(m_0 - m_1)$. Thus the decoded bit sequence are the same for the two methods.

Fig. 5 shows the partitions ($S_{I,k}^{(0)}, S_{I,k}^{(1)}$) for the generic bit $b_{I,k}$ in the case of the 16-QAM constellation. As a consequence,

$$D_{I,k} = \frac{1}{4} \left\{ \min_{\alpha \in S_{I,k}^{(0)}} |y[i] - \alpha|^2 - \min_{\alpha \in S_{I,k}^{(1)}} |y[i] - \alpha|^2 \right\}$$

can be simplified as follows.

$$D_{I,1} = \begin{cases} -y_I[i], & |y_I[i]| \leq 2 \\ -2(y_I[i] - 1), & y_I[i] > 2 \\ -2(y_I[i] + 1), & y_I[i] < -2 \end{cases} \quad (11)$$

$$D_{I,2} = |y_I[i]| - 2. \quad (12)$$

The same observation holds for QPSK and 64-QAM constellations.

4. PERFORMANCE AND ANALYSIS

We simulate the six Reed-Solomon codes, convolutional codes, and concatenated codes with $\alpha = 60$ and $\beta = 60$ respectively in AWGN channel. We show simulation results of

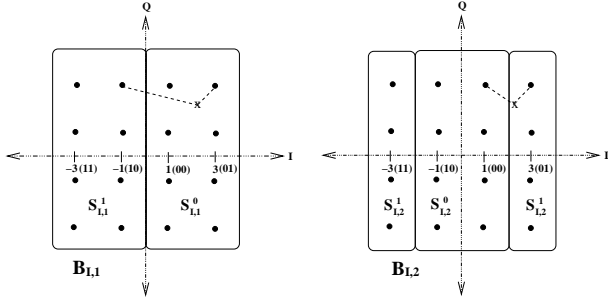


Fig. 5: Metric partitions of the 16-QAM constellation.

scheme 1 (QPSK), 3 (16QAM), and 5 (64QAM) in Fig. 6; other schemes have similar simulation results. The axes present energy per information bit (E_b/N_0) and information bit error rate (BER). The coding gains are obtained from reduction E_b/N_0 in coded BER curve compared to the curve of uncoded transmission with coherent demodulation.

We find that in AWGN channel, the performance of the concatenated code is worse than a single CC code under low E_b/N_0 . We conjecture that the reason is, the errors exceed the correction capability of outer RS code under low E_b/N_0 , yet the codeword energy of the concatenated code is inverse of RS code rate times of a single CC code.

Table 4 lists coding gains of the six concatenated codes obtained from simulation at $\text{BER}=10^{-6}$. Comparing with the theoretic coding gains based on minimum codeword distance in Table 2, we find the RS coding gains are less than the theoretic values by 2 to 3.5 dB and the CC coding gains are less than the theoretic values by 1 dB, which means that our low-complexity tail-biting suboptimal decoder have good performance and BICM mechanism only have little impact on the CC code. However, the overall coding gains under low E_b/N_0 are far away from the theoretic values, and we conjecture that the performance will more achieve above values under high E_b/N_0 .

5. CONCLUSION

In this paper, we designed the decoding algorithm for the shortened and punctured RS codes and proposed a low-complexity decoder for the tail-biting punctured CC codes under the BICM arrangement. From the simulation results in AWGN channel, we found that the coding gains of the RS codes and the CC codes almost achieved the theoretic values calculated based on minimum codeword distances, which means that our low-complexity suboptimal tail-biting decoder has good performance and the BICM mechanism only has little impact on the CC decoding performance. The performance of the concatenated codes is worse at the E_b/N_0 considered. We conjecture that their performance will also approach the

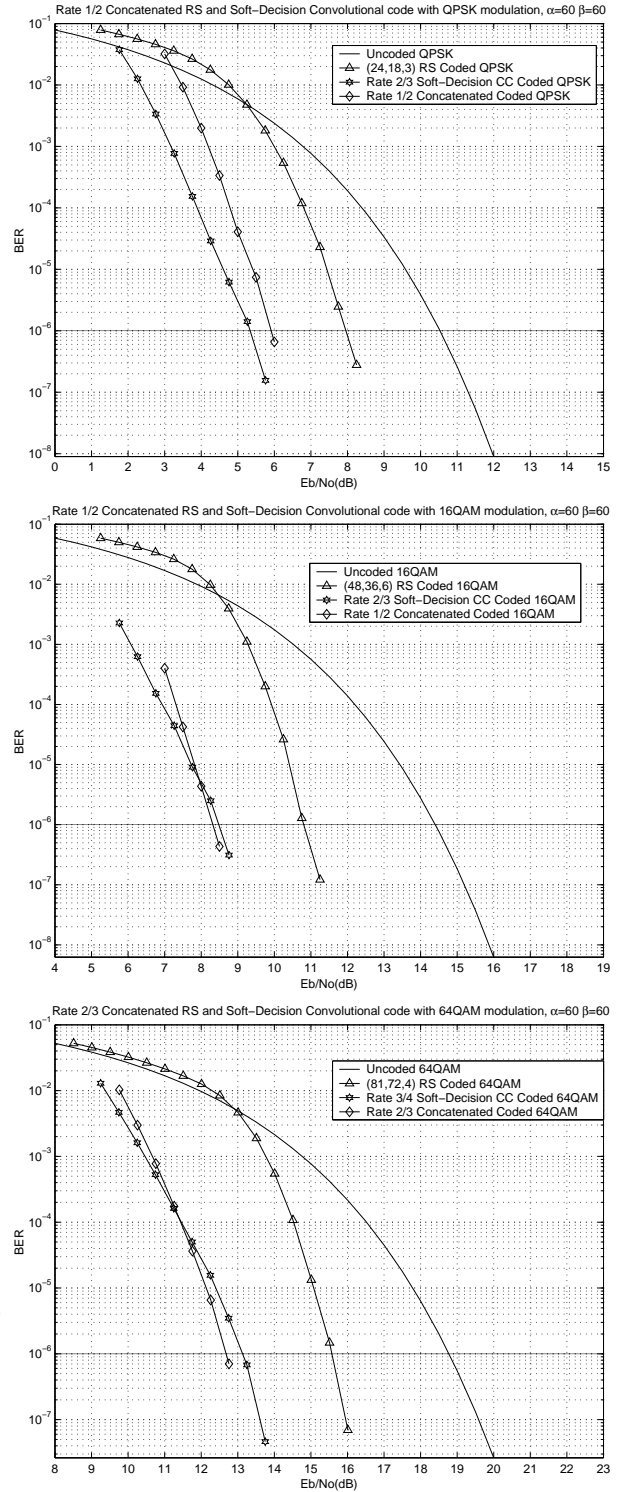


Fig. 6: Concatenated code performance in AWGN.

Table 4: Coding Gain from Simulation, in AWGN at BER = 10^{-6}

Scheme	RS Coding Gain from Simulation (dB)	Soft-Decision CC Coding Gain from Simulation (dB)	Concatenated Coding Gain from Simulation (dB)
1	2.57	5.19	4.62
2	2.24	4.19	3.62
3	3.6	5.9	6.04
4	2.9	4.43	4.38
5	3.24	5.62	6.04
6	3.19	4.9	5.1

theoretic values at high E_b/N_0 . These results can provide a basis for various further studies. For example, they can be used in guiding the work towards a practical hardware implementation.

6. REFERENCES

- [1] IEEE Std 802.16a-2003, *IEEE Standard for Local and Metropolitan Area Networks — Part 16: Air Interface for Fixed Broadband Wireless Access Systems — Amendment 2: Medium Access Control Modifications and Additional Physical Layer Specifications for 2–11 GHz*. New York: IEEE, April 2003.
- [2] I. S. Reed and X. Chen, *Error-Control Coding for Data Network*. Boston: Kluwer Academic Publishers, 1999.
- [3] H. H. Ma and J. K. Wolf, “On tail biting convolutional codes,” *IEEE Trans. Commun.*, vol. 34, pp. 104–111, 1986.
- [4] Y.-P. E. Wang and R. Ramésh, “To bite or not to bite — a study of tail bits versus tail-biting,” in *Proc. IEEE Int. Symp. Personal Indoor Mobile Radio Commun.*, vol. 2, pp. 317–321, Oct. 1996.
- [5] W. Sung and I.-K. Kim, “Performance of a fixed delay decoding scheme for tail biting convolutional codes,” in *IEEE Asilomar Signals Sys. Computers Conf. Rec.*, vol. 1, pp. 704–708, Oct. 1996.
- [6] E. Zehavi, “8-PSK trellis codes for a Rayleigh channel,” *IEEE Trans. Commun.*, vol. 40, pp. 873–884, May 1992.
- [7] M. Speth, A. Senst, and H. Meyr, “Low complexity space-frequency MLSE for multi-user COFDM,” in *IEEE Global Telecommun. Conf. Rec.*, vol. 5, pp. 2395–2399, 1999.
- [8] F. Tosato and P. Bisaglia, “Simplified soft-output demapper for binary interleaved COFDM with application to HIPERLAN/2,” in *IEEE Int. Conf. Commun. Conf. Rec.*, vol. 2, pp. 664–668, 2002.
- [9] J. G. Proakis, *Digital Communication, 4th ed.* New York: McGraw-Hill, 2001.
- [10] S. Lin and D. J. Costello, Jr., *Error Control Coding — Fundamentals and Applications*. New Jersey: Prentice-Hall, 1983.
- [11] C.-Y. Chen, “Software implementation and performance analyses for cable modem FEC code,” M.S. thesis, Department of Electrical Engineering, Chung Hua University, Hsinchu, Taiwan, R.O.C., June 2000.
- [12] D. W. Lin, *Digital Communication*. Course notes, Department of Electronics Engineering, National Chiao Tung University, Hsinchu, Taiwan, R.O.C., Fall 2000.